JTTEE5 13:200-213
DOI: 10.1361/10599630419337
1059-9630/$19.00 © ASM International

Peer Reviewed

Numerical Modeling of In-Flight Characteristics of Inconel 625 Particles During High-Velocity Oxy-Fuel Thermal Spraying

S. Gu, D.G. McCartney, C.N. Eastwick, and K. Simmons

(Submitted 24 December 2002; in revised form 7 April 2003)

A computational fluid dynamics (CFD) model is developed to predict particle dynamic behavior in a high-velocity oxyfuel (HVOF) thermal spray gun in which premixed oxygen and propylene are burnt in a combustion chamber linked to a long, parallel-sided nozzle. The particle transport equations are solved in a Lagrangian manner and coupled with the two-dimensional, axisymmetric, steady state, chemically reacting, turbulent gas flow. Within the particle transport model, the total flow of the particle phase is modeled by tracking a small number of particles through the continuum gas flow, and each of these individual particles is tracked independently through the continuous phase. Three different combustion chamber designs were modeled, and the in-flight particle characteristics of Inconel were 625 studied. Results are presented to show the effect of process parameters, such as particle injection speed and location, total gas flow rate, fuel-to-oxygen gas ratio, and particle size on the particle dynamic behavior for a parallel-sided, 12 mm long combustion chamber. The results indicate that the momentum and heat transfer to particles are primarily influenced by total gas flow. The 12 mm long chamber can achieve an optimum performance for Inconel 625 powder particles ranging in diameter from 20 to 40 μm. At a particular spraying distance, an optimal size of particles is observed with respect to particle temperature. The effect of different combustion chamber dimensions on particle dynamics was also investigated. The results obtained for both a 22 mm long chamber and also one with a conical, converging design are compared with the baseline data for the 12 mm chamber.

Keywords CFD, gas dynamics, HVOF, particle modeling

1. Introduction

High velocity oxyfuel (HVOF) thermal spraying offers a promising technology to produce protective coatings, typically 200-500 μm thick, on the surfaces of engineering components. Materials being sprayed include metallic alloys, cermets, ceramics, and polymers. In the HVOF process, oxygen and fuel are mixed and burnt in a combustion chamber at high flow rates and pressures to produce a high-temperature, high-speed gas jet. Powder particles, normally in the size range 5-65 μm, are injected into the gas jet so that they are heated as they are accelerated toward the substrate to be coated. On arrival at the substrate, particles are ideally in a melted or softened state and, on impact, form lenticular splats, which adhere well to the substrate and to one another. The HVOF gun is scanned cross the substrate to build up the required coating thickness in a number of passes.

The properties of a thermally sprayed coating are strongly influenced by the microstructure of the deposit and the phases formed within it. These, in turn, will be directly determined by the process parameters, such as fuel-to-oxygen ratio, total gas flow rate, standoff distance between gun and substrate, powder particle size range and powder particle properties.

In HVOF spraying, the feedstock powder has a density three or four orders of magnitude greater than the gas density; its other

S. Gu, School of Engineering and Applied Science, Aston University, Aston Triangle, Birmingham B4 7ET, United Kingdom; **D.G. McCartney, C.N. Eastwick,** and **K. Simmons,** School of Mechanical, Materials, Manufacturing Engineering and Management, University of Nottingham, University Park, Nottingham NG7 2RD, United Kingdom. Contact e-mail: s.gu@aston.ac.uk.

Table of Symbols

A_p	surface area of the particle, m^2
Bi	biot number
$C_{p\text{-}g}$	specific heat of the gas, J $kg^{-1}K^{-1}$
$C_{p\text{-}p}$	specific heat of the particle, J kg^{-1} K^{-1}
d_p	diameter of the particle, m
F	force, N
F_D	drag force, N
h	heat transfer coefficient, W m^{-2} K^{-1}
m_p	mass of the particle, kg
Nu	Nusselt number
Re	Reynolds number
Pr	Prandtl number
T_g	temperature of the gas, K
T_p	temperature of the particle, K
t	time, s
v_g	velocity of the gas, m s^{-1}
v_p	velocity of the particle, m s^{-1}
λ_g	thermal conductivity of the gas, W m^{-1} K^{-1}
λ_p	thermal conductivity of the particle, W m^{-1} K^{-1}
μ_g	dynamic viscosity of the gas, kg m^{-1} s^{-1}
ρ_g	density of the gas, kg m^{-3}
ρ_p	density of the particle, kg m^{-3}

thermophysical properties are also significantly different from those of gas. Therefore, the involvement of powder in the HVOF simulation needs to be treated as a multiphase flow problem. Two approaches have been generally used to solve the multiphase flow: the Euler-Euler approach and the Euler-Lagrange approach.

In the Euler-Euler approach, the different phases are treated mathematically as interpenetrating continua. Since the volume of a phase cannot be occupied by the other phases, the concept of phase volume fraction is introduced. These volume fractions are assumed to be continuous functions of space and time and their sum is equal to one. Conservation equations for each phase are derived to obtain a set of equations that have similar structure for all phases.[1] This approach is appropriate for the modeling of liquid-liquid mixtures or any application where the volume fraction of the second phase is not negligible. In the Euler-Lagrange approach, the fluid phase is treated as a continuum by solving the time-averaged Navier-Stokes equations, while the dispersed phase behavior is solved by tracking a large number of particles through the calculated flow field. The dispersed phase can exchange momentum, mass, and energy with the fluid phase. A fundamental assumption made in the Euler-Lagrange approach is that the dispersed second phase occupies a low volume fraction (< 10%).[1] The particle trajectories are computed individually at specified intervals during the fluid phase calculation. The assumption can be made that the powder phase is sufficiently diluted that particle-particle interactions and the effects of the particle volume fraction on the gas phase are negligible.

The Euler-Lagrange approach has been used for the modeling of particle-gas interaction in various HVOF thermal spray systems. Power et al.[1] and Smith et al.[2] adopted this approach to simulate gas and particle flow in a Sulzer-Metco Diamond Jet (Sulzer Metco AG, Wohlen, Switzerland) (DJ) gun. The evolution of particle dynamics and the effects of process parameters were examined thoroughly in terms of velocity, temperature and trajectories. Oberkampf et al.[3,4] modeled copper particles also in a DJ gun, using Lagrange particle tracking algorithms. A comparison was given for the velocity and temperature development of the particles at different sizes. Lopez et al.[5,6] developed a 3D numerical model for Sulzer Metco Diamond Jet Rotating Wire (DJRW) system. They also predicted particle velocities using a Lagrange particle-tracking model and found results to be in reasonable agreement with laser two-focus velocimetry measurements. Yang et al.[7] used a decoupled Euler-Lagrange approach to simulate the gas flow field and in-flight particle behavior in a liquid-fueled HVOF gun similar to the JP-5000 system (Praxair & Tafa Thermal Spray Products, Praxair Surface Technology, Inc., Indianapolis, IN). The particle model was validated by experimental measurement of the particle velocity and excellent agreement was obtained between simulations and measurements.

In a previous paper,[8] the present authors detailed a numerical model of gas flow in a HVOF gun similar in design to a HV2000 (Praxair Thermal Spray Products). This work revealed the complexity of the gas dynamics involved, such as fuel gas combustion, supersonic free jet expansion and turbulent flow interaction. The parametric study described therein demonstrated the dependency of gas dynamic behavior on total gas flow rate, fuel-to-oxygen gas ratio, and the size and design of the combustion chamber. However, a particle model needs to be established to examine in detail the effects of gas dynamics on in-flight particle behavior.

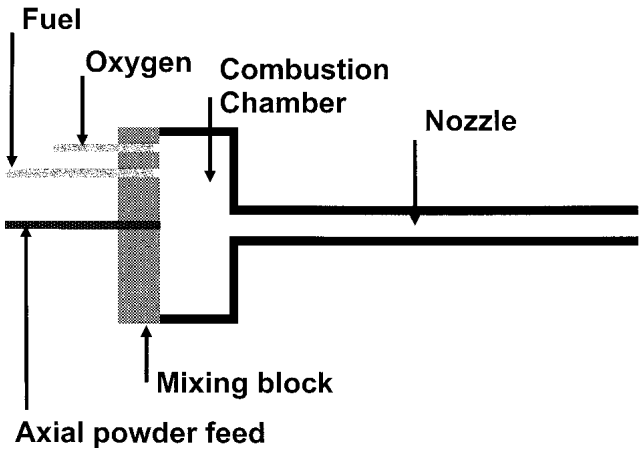

Fig. 1 Schematic representation of the HVOF gun geometry, showing premixed fuel and oxygen entering the combustion chamber, which is connected to a parallel-sided nozzle.

The numerical study of particle behavior can be divided into two phases: a macroscopic motion and heating model of the particle interacting with the gas flow and a microscopic heat transfer model for the particle where melting, vaporization and resolidification are taken into account. The purpose of the current study is to integrate a macroscopic particle model with the gas dynamic analysis previously described[8] using the Euler-Lagrange approach in which the particles are assumed to have a negligible effect on the gas flow field. This paper presents the results of particle motion and heating within the gas flow field and investigates the effect of changes in process parameters. In addition, the effect of modified combustion chamber designs is reported. The microscopic behavior of particle melting and resolidification will be addressed in a future publication.

2. Computational Model

2.1 System Geometry

A schematic representation of the gun with a nominal 12 mm combustion chamber length as specified by the manufacturer is shown in Fig. 1 and the dimensions are described in Table 1. Oxygen and propylene are injected into the water-cooled combustion chamber, through an annular array of fine orifices, where the gases burn and the combustion products are accelerated down the parallel-sized nozzle. Powder particles are injected axially into the combustion chamber by a carrier gas flow. The particle-laden gas mixture then exits the nozzle at a high temperature and velocity toward the substrate to be coated.

2.2 Model Description and Simplifications

The computational particle model is coupled with the previous gas dynamic model, which is represented as a compressible and turbulent chemically reacting flow.[8] The two-dimensional, axisymmetric simulations are performed in the commercially available finite volume CFD code CFX 4.2.[9] The computational geometry and boundary conditions were described in de-

Table 1 Dimensions of the Principal Components of the HVOF Gun Shown in Fig. 1

Component	Dimension/mm
Combustion chamber (nominal 12 mm size)	14 by 23.7 (length by diameter)
Nozzle	115 by 7.7 (length by diameter)
Powder/carrier gas injector	1.1 (diameter)
Fuel/oxygen injector	0.9 (annular width)

Table 2 Process Parameters for Baseline Computational Calculations Within 12 mm Combustion Chamber

C_3H_6 Flow Rate (Fuel), SCFH	O_2 Flow Rate, SCFH	N_2 Flow Rate (Carrier Gas), SCFH	Particle Flow Rate, g s^{-1}
150	555	35	0.556
125	465	35	0.556

Table 3 Chemical Composition of the Inconel 625 Powder (wt.%)

Ni	Cr	Mo	Nb	Fe	Ti	Al	C	N	O
66.5	20.6	8.99	3.55	0.045	0.012	0.24	0.006	0.075	0.015

tail previously.[8] Briefly, there are 1000 cells within the 12 mm combustion chamber, 3500 cells in the nozzle section, and 7300 cells outside the gun. Grid sensitivity studies were carried out by doubling the cell number both axially and radially and the numerical solutions from both meshes were almost identical. The process parameters used in the computational modeling are listed in Table 2. Values are given in standard cubic feet per hour (SCFH), as this the practical unit used on control consoles for this gun system. Appendix Table A1 provides conversion factors to other systems of units. The parametric data show that the powder mass flow rate is less than 10% of the total mass flow rate, thus the particle transport equations can, to a good approximation, be solved in a Lagrangian frame of reference. The powder is Inconel 625 of composition given in Table 3. The powder is treated as comprising spherical particles, this assumption is close to the physical morphology of powder particles, as illustrated in Fig. 2.

It is generally accepted[10] that heat conduction within a particle can be neglected if Bi <0.02. In the present analysis, we shall assume this to be the case although the validity is examined in Sec. 3.1. The particle is therefore treated as isothermal.

The current study is focused on examining the effect of process parameters on macroscopic particle dynamics, not on a quantitative prediction of phase change processes. Hence, particles are treated as solid throughout the computational domain and phenomena such as particle melting, vaporization, and possible resolidification are ignored.

2.3 Computational Models

2.3.1 Momentum Transfer Equations. The momentum transport between the gas and particle can be solved directly from Newton's second law:

$$m_p \frac{dv_p}{dt} = F \qquad \text{(Eq 1)}$$

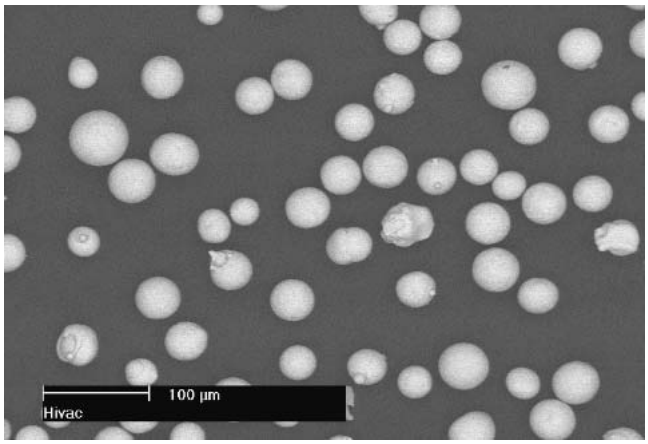

Fig. 2 Scanning electron microscope image of the external morphology of feedstock powder showing spherical geometry

The acting force in the particle could involve the drag force, force due to pressure gradients, force due to added mass, Basset history term, and external potential forces.[10] In principle, among the factors that affect the movement of particle during the HVOF process, only the drag force plays a dominant role, other factors can be neglected in most cases.[10] Therefore, the aerodynamic drag force can be used to represent the general force in the form:

$$F_D = \frac{1}{8} A_p \rho_g C_d \mid v_g - v_p \mid (v_g - v_p) \qquad \text{(Eq 2)}$$

The acceleration for a spherical particle is deduced as

$$\frac{dv_p}{dt} = \frac{3\rho_g}{4 d_p \rho_p} C_d \mid v_g - v_p \mid (v_g - v_p) \qquad \text{(Eq 3)}$$

The drag factor C_d is given by

$$C_d = \frac{24}{Re} \qquad (Re < 1)$$

$$C_d = \frac{24}{Re}(1 + 0.15\, Re^{0.67}) \qquad (1 < Re < 10^3) \qquad \text{(Eq 4)}$$

$$C_d = 0.44 \qquad (Re > 10^3)$$

The Reynolds number is defined by

$$Re = \frac{\rho_g \mid v_g - v_p \mid d_p}{\mu_g} \qquad \text{(Eq 5)}$$

2.3.2 Heat Transfer Equations. In the thermal spray process, the radiation heat loss from the particle to the surroundings are negligible compared with the convective heat flux from the gas to the particle.[11] Therefore, particle heating (neglecting latent heat effects) is given by

$$m_p C_{p-p} \frac{dT_p}{dt} = h(T_g - T_p) A_p \qquad \text{(Eq 6)}$$

The heat transfer coefficient h is given by

$$h = \mathrm{N}u\lambda_g/d_p \quad \text{(Eq 7)}$$

The Nusselt number is given by

$$\mathrm{N}u = 2 + 0.6Re^{0.5}\,Pr^{1/3} \quad \text{(Eq 8)}$$

The Prandtl number of the gas is defined as

$$Pr = \mu_g C_{p-g}/\lambda_g \quad \text{(Eq 9)}$$

The heating rate of the particle is then obtained from

$$\frac{dT_p}{dT} = \frac{6\lambda_g(2 + 0.6Re^{0.5}\,Pr^{1/3})(T_g - T_p)}{d_p^2\rho_p C_{p-p}} \quad \text{(Eq 10)}$$

3. Computational Results and Discussion

3.1 Parametric Study

The results presented in this section are based on the gun design within a 12 mm long parallel sided combustion chamber (Fig. 1) under operating conditions of a total gas flow rate, 705 SCFH, and fuel-to-oxygen volume flow ratio, 0.27, i.e., 125 SCFH propylene and 465 SCFH oxygen.

3.1.1 Influence of Particle Injection Velocity. The particle injection velocity can be manipulated by carrier gas flow rate and typically varies in the range 10-100 m/s.[12] In this calculation, a 25 μm diameter Inconel 625 particle is injected at the center of the axially located injection orifice with a mass flow rate of 0.556 g/s. The injection velocities are given the values of 20, 40, 60, and 80 m/s. Figure 3(a) illustrates the influence of the injection velocity on the particle temperature evolution. A threefold increase of particle injection speed from 20-80 m/s only results in a maximum temperature reduction from 1900-1800 K at an axial distance of 0.17 m, due to the reduction of particle dwell time. It should be noted that the monotonic rise of particle temperature, shown after crossing the melting point, is a computational phenomenon caused by the neglect of latent heat in the particle model, i.e., particle melting is neglected. The results in Fig. 3(b) show that the change of particle injection speed has virtually no effect on the evolution of particle velocity. The small influence of injection velocity on particle motion and heating history predicted by this particle modeling is consistent with the prediction made by Shrikant et al.[12] This feature may be attributed to the uniform heat input and acceleration within HVOF systems; thus, the small variation in the particle dwell time that is brought about by changing the injection velocity has little effect on HVOF spraying for this range of velocities.

3.1.2 Influence of Particle Injection Position. This HVOF gun is designed to introduce the spray powder uniformly into the center of the combustion chamber through an axially located injection hole with a radius of 0.55 mm. In this calculation, 25 μm Inconel 625 particles are released from six separate positions along a radius of the injection hole, with a total mass flow rate of 0.556 g/s. Each particle is injected at a speed of 20 m/s representing a mass flow rate of 0.0927 g/s. The injection locations are 0, 0.1, 0.2, 0.3, 0.4, and 0.5 mm from the hole's center in the radial direction. The predicted paths for these particles plotted in Fig. 4(a) show that the particles start to spread at the injection points, the spreading peaks before the nozzle entrance, and the particles converge towards the centerline in the nozzle and the free jet region. The outermost particle has the highest spreading rate while the center particle essentially travels along the centerline of the gun. The sharp convergence of particle trajectories around the nozzle entrance is due to the strongly convergent gas flow field at the nozzle entrance.[8] The outermost particles cross the centerline of the gun after the nozzle exit, which suggests a possible particle interaction in that region. However, even in the case of the outmost particle, spreading is less than 10% of the central hole radius. Therefore all the particles are nearly collinear with the centerline of the gun during flight. The particle temperature profiles in Fig. 4(b) demonstrate greater heating for the outmost particle, which could be explained by having more contact with the hot gas stream in the recirculation region within the combustion chamber as revealed by the calculations previously reported.[8] The results also demonstrate the particle velocity evolution is insensitive to the injection location as shown in Fig. 4(c).

3.1.3 Influence of Total Gas Flow Rate and Gas Ratio. In this calculation, two total gas flow rates were considered, namely 705 and 590 SCFH, at each of these flow rates, and two fuel-to-oxygen ratios, namely 0.248 and 0.322, were investigated. These correspond to 89% and 69%, respectively, of the stoichiometric oxygen requirements. The 25 μm computational particle is fed through the center of the injection hole at speed of 20 m/s with a mass flow rate of 0.556 g/s. The effects of gas flow rate and ratio on velocity evolution of the particle are shown in Fig. 5(a). The particle gains more momentum at the higher gas flow rate and higher fuel-to-oxygen ratio. The positive linear correlation between particle velocity and fuel-to-oxygen ratio is illustrated in Fig. 5(b) where additional fuel-to-oxygen ratios has been compared. The temperature profiles in Fig. 5(c) show that more heat is transferred to the particle at higher flow rate, while the variation of fuel-to-oxygen ratio has negligible effect on particle temperature as revealed by the overlap of plotted points. Therefore, to achieve greatest velocity, for a given maximum particle temperature a more fuel rich flame should be used (69% stoichiometry).

3.1.4 Influence of Particle Size. Feedstock powder is generally supplied with a certain defined size range. This study also examined the effect of different particle sizes on particle behavior to provide information on the optimum range within the nominal size distribution. In these calculations, different sized Inconel 625 particles ranging from 10 to 60 μm were injected at the center of the injection hole with a speed of 20 m/s, representing a mass flow rate of 0.556 g/s in each case. Figure 6(a) shows particle velocity as a function of axial distance, the previously reported gas velocity is also presented for comparison. It is seen that the small particles are accelerated more throughout the computational domain. When the particle velocity is higher than the gas velocity, as the gas jet decays outside the gun, the drag force on the particle then changes direction and becomes a resistance to the particle motion. The velocity of the particle is then de-

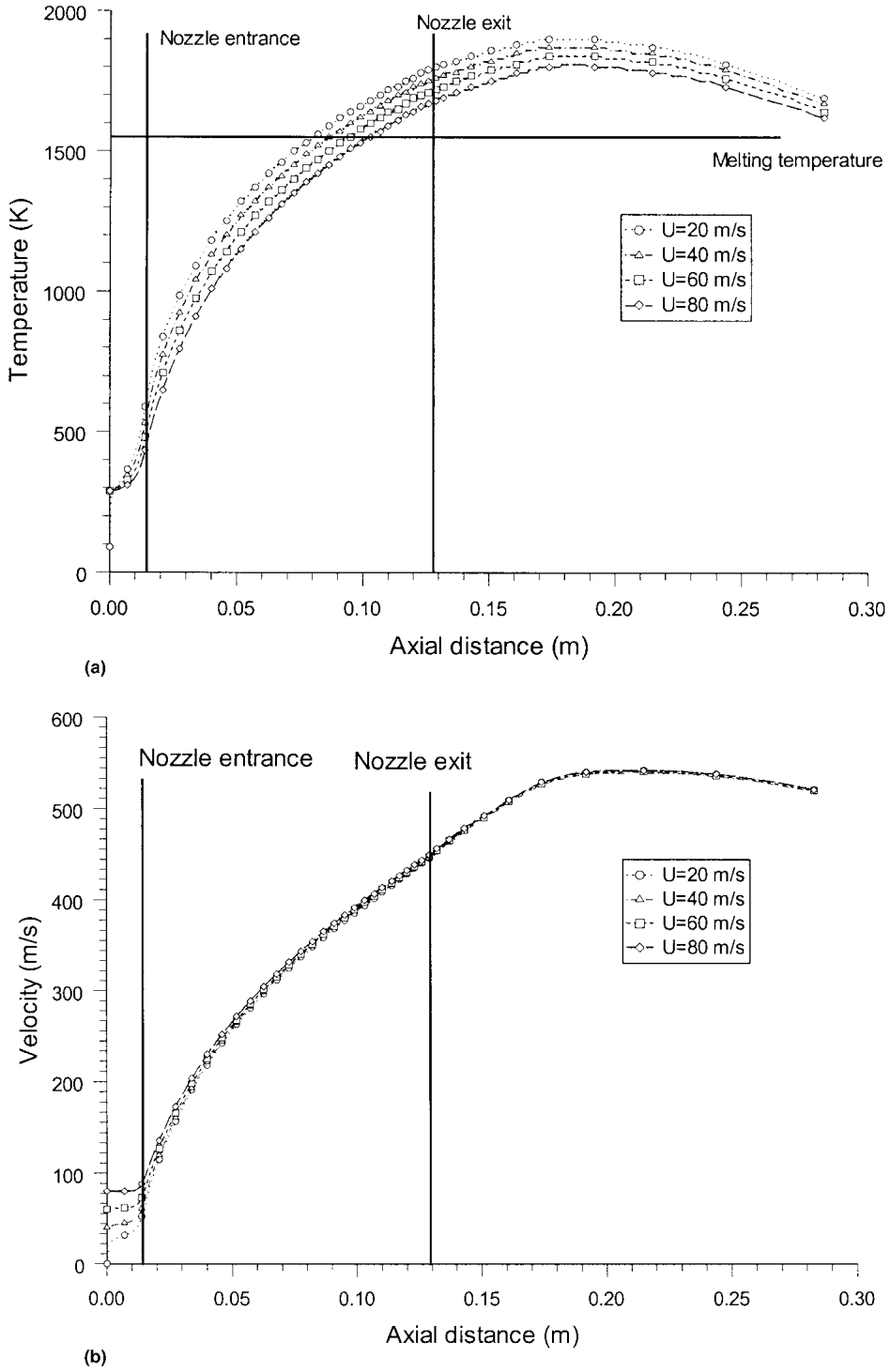

Fig. 3 **(a)** Evolution of particle temperature versus axial distance for different particle injection speeds (25 μm diameter particle). **(b)** Evolution of particle velocity versus axial distance for different particle injection speeds (25 μm diameter particle).

creased. The smaller the particle size, the more easily it is decelerated. A larger particle, on the other hand, has greater ability to maintain its velocity during the deceleration stage, due to its larger inertia. The velocity decrease with respect to particle size is more clearly demonstrated in Fig. 6(b), which is a plot of particle velocity versus particle diameter at various distances from the end of the nozzle. It is evident that the velocity of particles is strongly dependent on their size when the particle is smaller than 30 μm, whereas the dependency is less pronounced for particles larger than 30 μm.

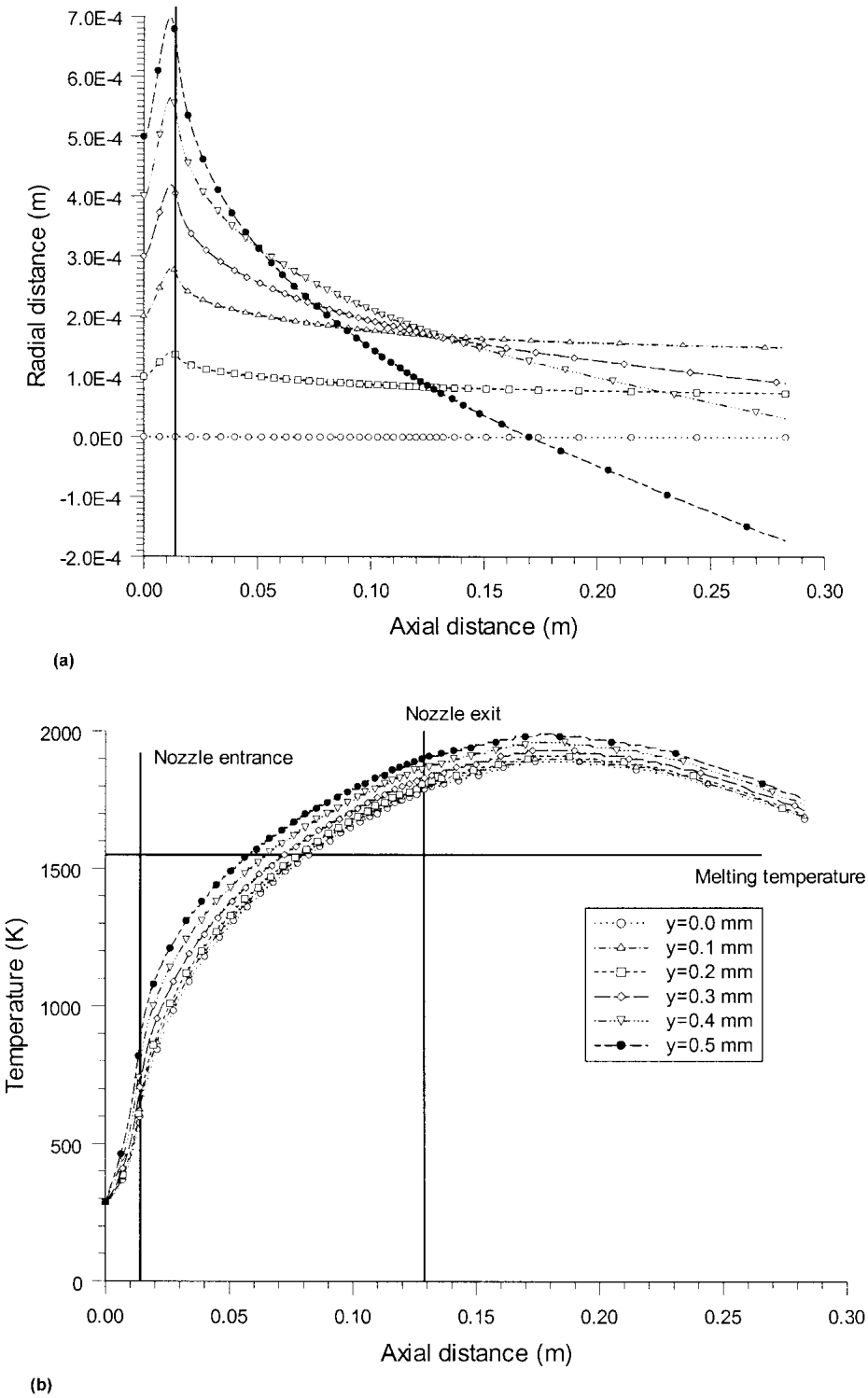

Fig. 4 **(a)** Particle trajectory for different injection locations (25 μm diameter particle). Initial positions are 0, 0.1, 0.2, 0.3, 0.4, and 0.5 mm from the axis. The vertical line represents the nozzle entrance. The nozzle exit is at 0.13 m. **(b)** Evolution of particle temperature versus axial distance for different injection locations (25 μm diameter particle); *y* is the distance of the injection location from the axis.

The temperature developments are illustrated in Fig. 6(c). The results show that for a melting point of 1563 K (i.e., that of Inconel 625), particles smaller than 20 μm will be greatly overheated leading to undesirable oxidation reactions as reported by Edris et al.[13] Particles larger than 50 μm may never achieve the desired liquid state during the process. The relationship between

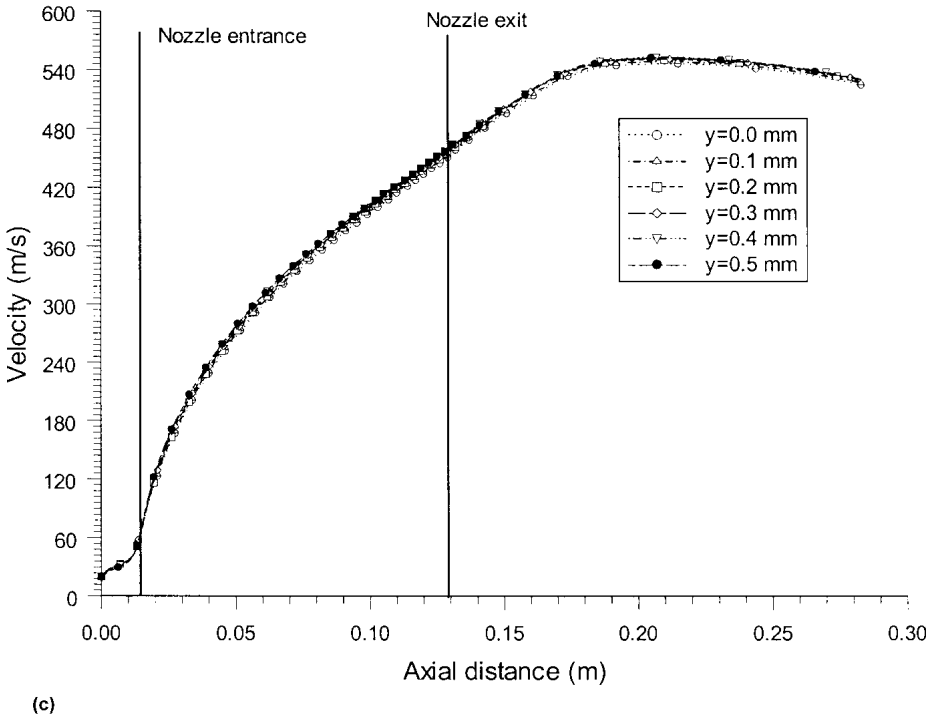

(c)

Fig. 4 cont. **(c)** Evolution of particle velocity versus axial distance for different injection locations (25 μm diameter particle); *y* is the distance of the injection location from the axis.

Table 4 Thermophysical Properties Assumed for Inconel 625

Density, kg m^{-3}	Relative Atomic Mass, kg mol^{-1}	Melting Point, K	Specific Heat, J kg^{-1} K^{-1}	Thermal Conductivity, W m^{-1} K^{-1}
8440	0.0618	1560	410	9.8

the particle temperature and size is illustrated in Fig. 6(d) for various distances from the end of the nozzle. It is noticed that an optimum size of particles is observed to be around 20-40 μm, which is in reasonable agreement with practical experience. Note, however, that in the present calculation latent heat absorption, i.e., particle melting is neglected.

The results are consistent with a number of existing particle models in HVOF spraying[1-7] and confirm that the momentum and heat exchanges between small particles and gas flow are proportionately greater. As a result, small particles are accelerated and heated sufficiently, whereas large particles are not during the spray process.

From the results, we can now discuss the validity of the assumption that $Bi < 0.03$. The heat transfer coefficient h can be deduced from Eq 7-9. Using the gas and particle data based on the initial inputs from Tables 4 and 5, it is found that $Bi \sim 0.03$ for the Inconel 625 powder within the size range examined. We should therefore point out that a temperature gradient may exist within Inconel 625 powder particles that cannot be neglected in quantifying the microscopic aspects of particle melting. The fundamental reason for this is the value of the thermal conductivity of the alloy (9.8 Wm^{-1}K^{-1}) that is low in comparison with many metals and other alloys.

Table 5 Thermophysical Parameters Used in the Computations. Gas Properties, Apart From Viscosity, Are Treated as Pressure and Temperature Dependent in Calculations

Parameters	Value
C_{p-g}	1040 J kg^{-1} K^{-1}
C_{p-p}	410 J kg^{-1} K^{-1}
T_g	288 K (Initial temperature)
T_p	288 K (Initial temperature)
ω_g	315 m s^{-1} (Initial injection velocity)
ω_p	20 m s^{-1} (Initial injection velocity)
λ_g	0.02763 W m^{-1} K^{-1}
μ_g	1.81 × 10^{-5} kg m^{-1} s^{-1}
ρ_g	1.25053 kg m^{-3}
ρ_p	8440 kg m^{-3}

3.2 Design of Combustion Chamber

The effect of combustion chamber size and geometry is examined in this section. Specifically, additional combustion chambers of nominal lengths 22 and 3 mm, respectively, are considered. The computational geometries and gas dynamics for the above designs have been described in the previous paper[8] and schematic representations of the above combustion chamber designs are shown in Fig. 7. An important point to note is that the design referred to as the 3 mm chamber comprises a short 3 mm parallel sided section but a longer converging, conical section, thus the entrance to the nozzle is some 30 mm from the point of powder injection into the chamber. The objective of this analysis was to provide insight into the optimum combustion chamber selection for the spraying of specific materials. It is generally believed that a 22 mm chamber should be selected for higher

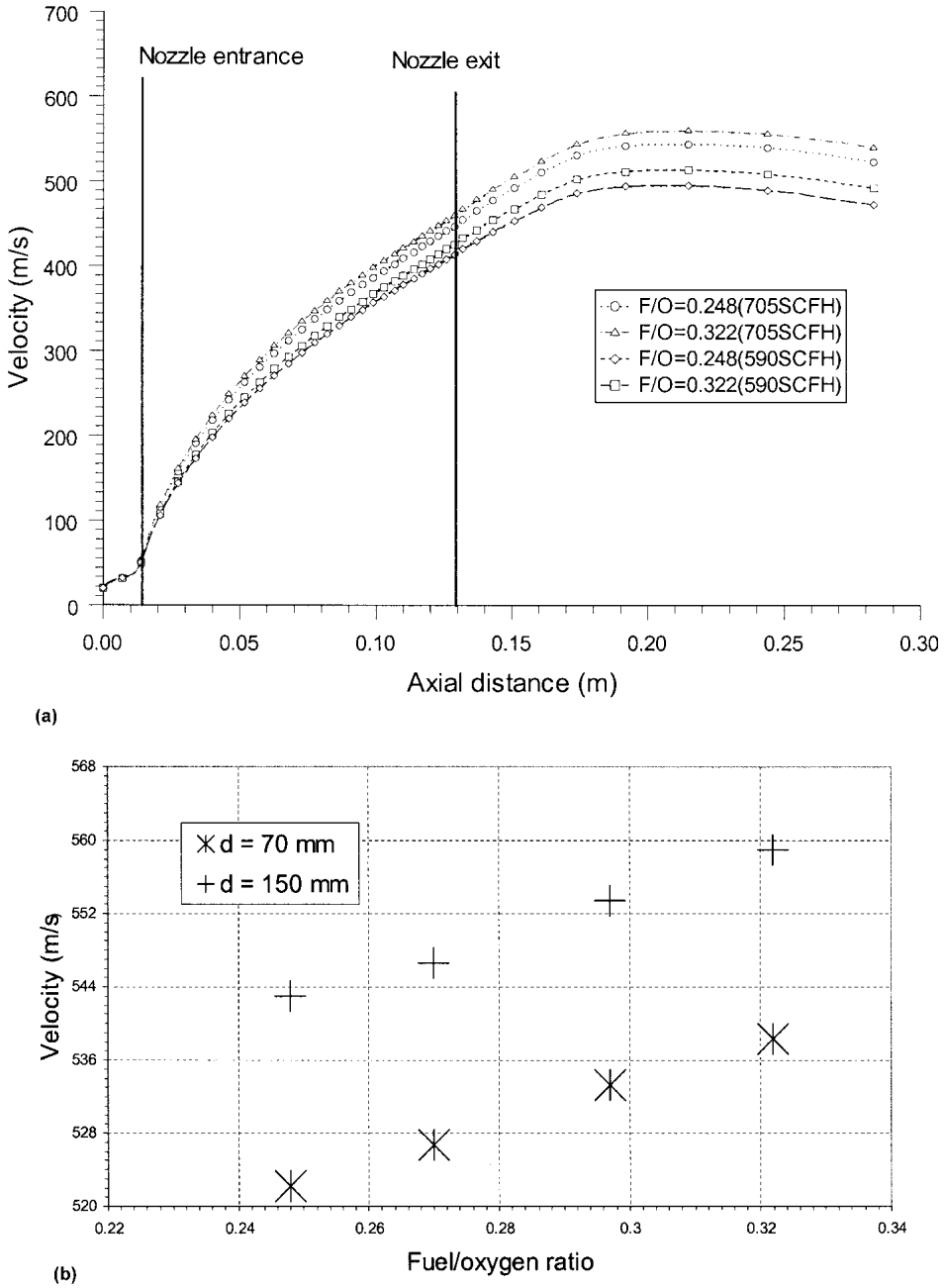

Fig. 5 **(a)** Evolution of particle velocity versus axial distance for different gas flow rates and ratios (25 μm diameter particle). F/O is fuel-to-oxygen volume flow ratio. **(b)** Evolution of particle velocity versus fuel-to-oxygen ratio at different distances from the nozzle exit (25 μm diameter particle); *d* is stand-off distances from the nozzle exit.

melting point materials and a 3 mm one used for materials of lower melting points. Thus, to make appropriate comparisons, the lower and upper total gas flow rates of 590 and 705 SCFH were used as the respective flow rates for the 3 and 22 mm chambers. The fuel-to-oxygen ratio was fixed at 0.27 in these calculations, i.e., 82% of the stoichiometric requirement. Inconel 625 particles of diameter 25 μm were used in the calculations for these different chamber designs. The particles were released at the center of the injection hole at a speed of 20 m/s, representing a mass flow rate of 0.556 g/s.

A comparison of particle velocity evolutions between the 12 and 22 mm chamber designs is given in Fig. 8(a). The gas dynamic study revealed a significantly lower gas velocity profile within the 22 mm combustion chamber,[8] and as a consequence, particles in the 22 mm chamber reach only about half the velocity value attained with the 12 mm chamber before entering the nozzle. However, the slower particle acceleration within the 22 mm chamber is almost entirely compensated in the nozzle and by the end of the computational domain both chamber designs achieve a similar particle velocity. With regard to the particle

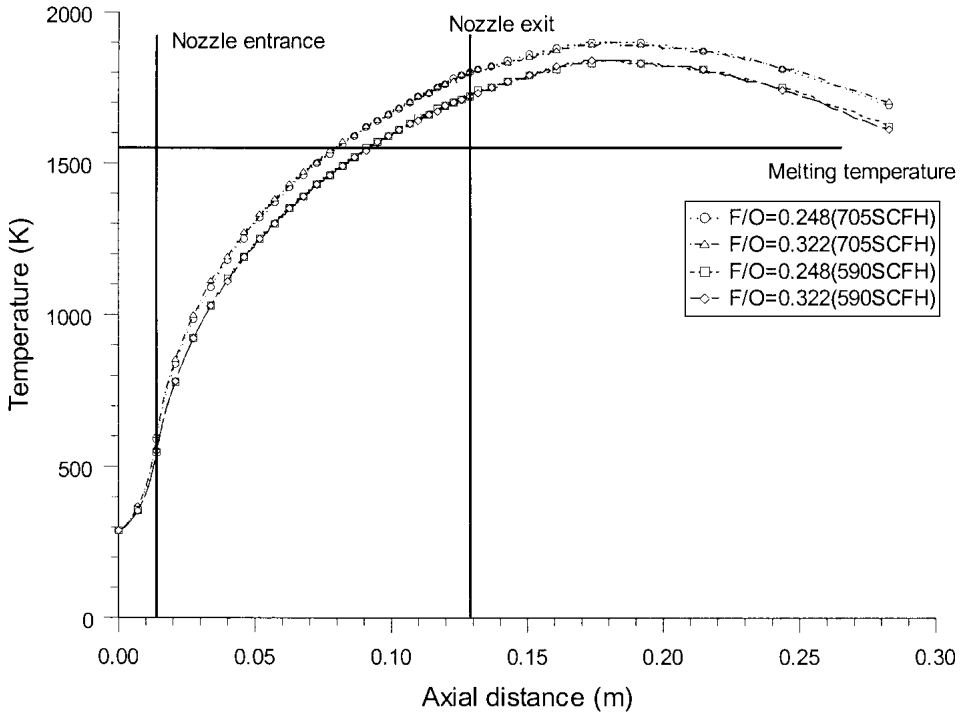

(c)

Fig. 5 cont. **(c)** Evolution of particle temperatures versus axial distance for different gas flow rates and ratios (25 μm diameter particle). F/O is fuel-to-oxygen volume flow ratio.

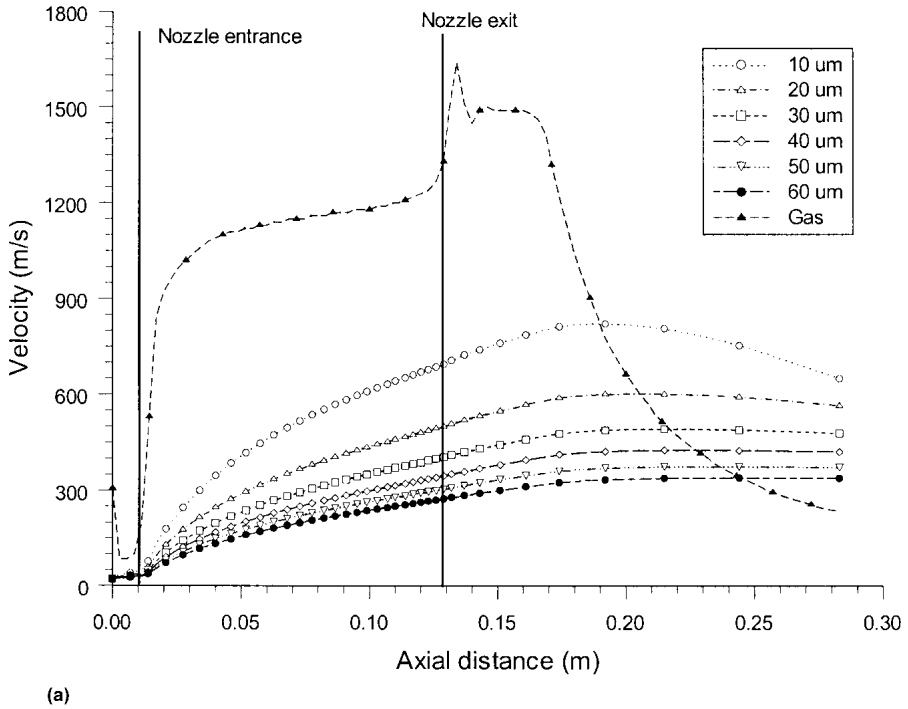

(a)

Fig. 6 **(a)** Evolution of particle velocity versus axial distance for different particle sizes.

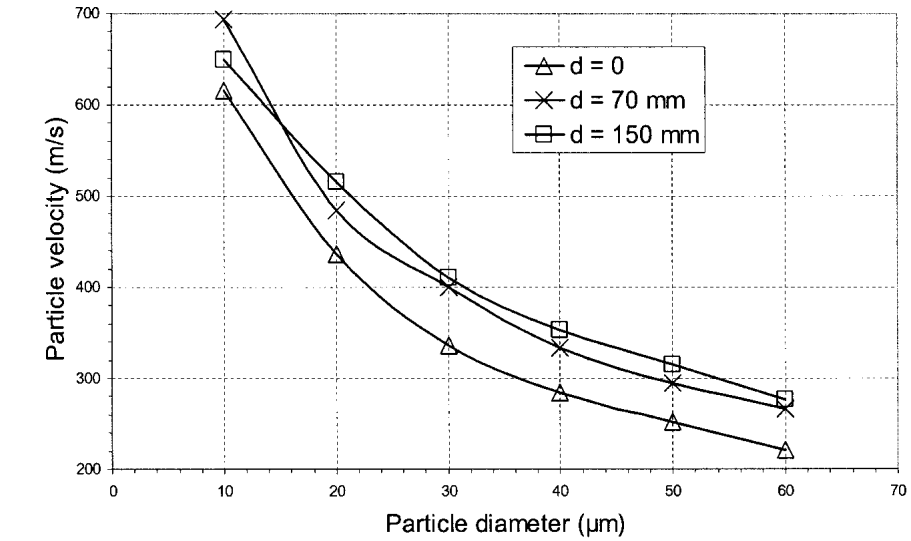

(b)

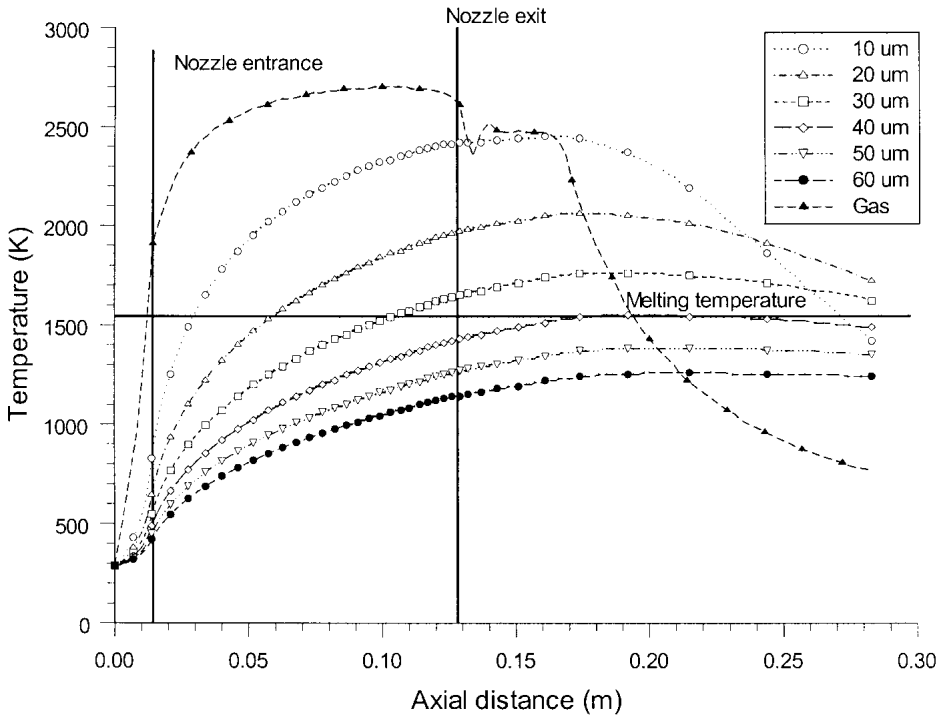

(c)

Fig. 6 cont. **(b)** Evolution of particle velocity versus particle size at different distances from the nozzle exit. **(c)** Evolution of particle temperature versus axial distance for different particle sizes.

temperature, the relative behavior depicted in Fig. 8(b) demonstrates the increased particle temperature arising from the extended dwell time with the 22 mm design. The results above are generally confirmed by practical experience with this type of gun system where the 22 mm device is more generally applicable for higher melting point materials.

A comparison of particle velocity developments between the 12 and 3 mm chamber designs is provided in Fig. 9(a). The lower gas velocity, reported in the gas dynamic modeling[8] in the 3 mm chamber system, has a direct impact on the particle velocity evolution. The results of particle modeling demonstrate a markedly lower velocity profile throughout the 3 mm chamber and nozzle system. Additionally, the particle temperature profiles in Fig. 9(b) confirm the implication from the gas dynamic study that the 3 mm chamber design produces greater particle heating than the 12 mm chamber design. This prediction seems to be contrary to the general recommendation to use the 3 mm design for the spraying of low melting point materials. However, it is also found, by examining the flow patterns within the 3 and 12 mm combustion chambers,[8] that the gas flow con-

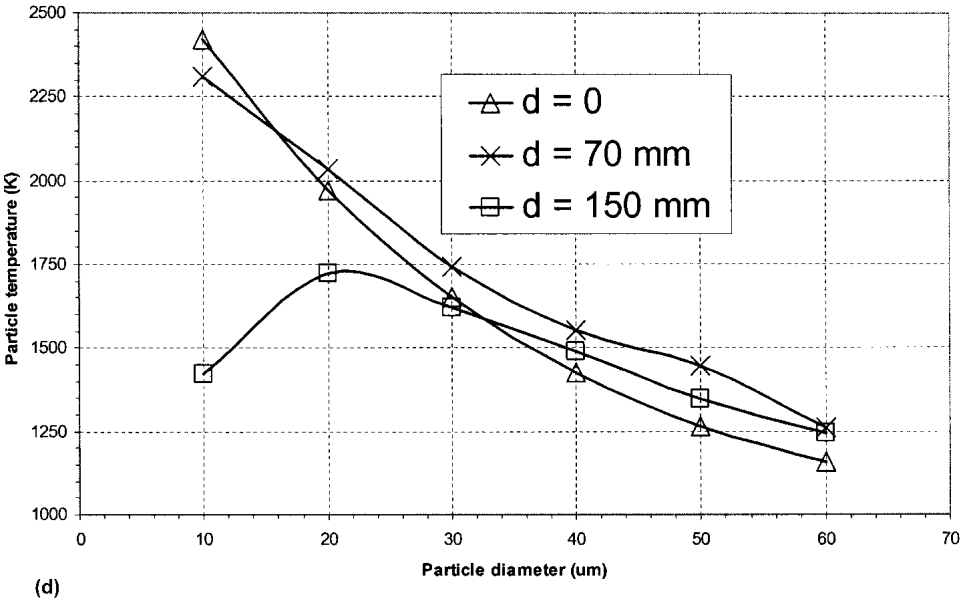

Fig. 6 cont. **(d)** Evolution of particle temperature versus particle size at different distances from the nozzle exit

verges towards the nozzle entrance more slowly in the 3 mm convergent, conical chamber design. One might thus speculate that this feature could effectively reduce the contact of particles with the internal surface of the gun and therefore avoid powder build up. This can be a major concern when spraying low melting point materials such as aluminium alloys and may be a significant factor in selecting the converging chamber over the parallel-sided one, despite the evident increase in thermal input to the powder.

4. Conclusions

A two-dimensional axisymmetric CFD model, using CFX, has been developed to investigate the particle dynamic behavior in an HV2000-type HVOF spray gun using the fuel propylene premixed with oxygen. The model used a Lagrangian particle tracking frame coupled with a steady-state gas flow field to examine particle motion and heating during HVOF spraying. The model was used to investigate the effects of process parameters and chamber design on in-flight particle behavior. The following conclusions have been obtained.

- An increase in particle injection velocity only slightly reduces the particle temperature development and has virtually no effect on the particle velocity profile. This feature is attributed to the relatively uniform heat input and acceleration within HVOF system; thus, the small variation in the particle dwell time that is brought about by changing the injection speed has little effect in HVOF spraying.
- The particle injected at the outermost radius from the center of the injection hole has the highest rate of spreading while the central particle essentially travels along the centerline of the gun. All the spreading particles converge towards the centerline of the gun after entering the nozzle and the trend continues till the end of the nozzle.

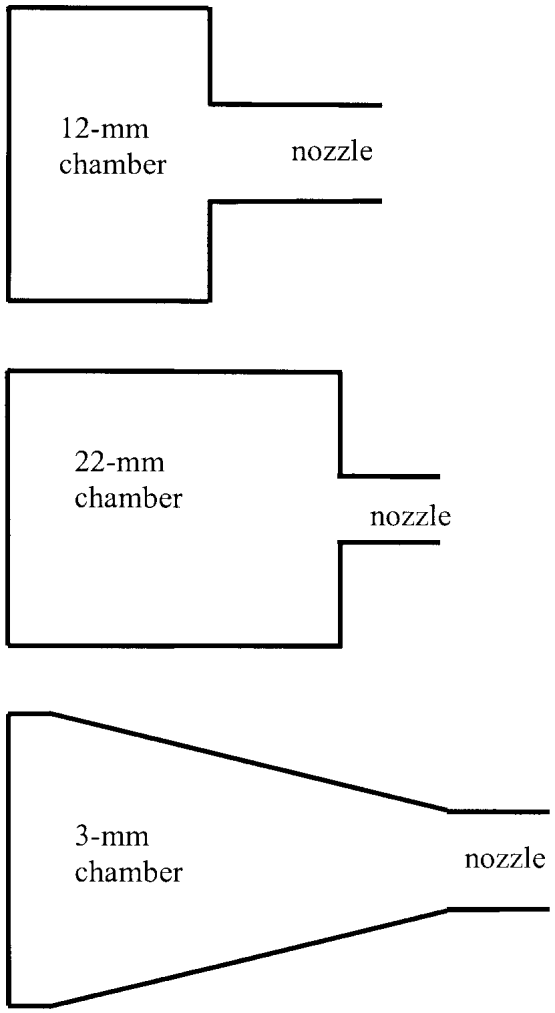

Fig. 7 Schematic representations of three different combustion chamber designs

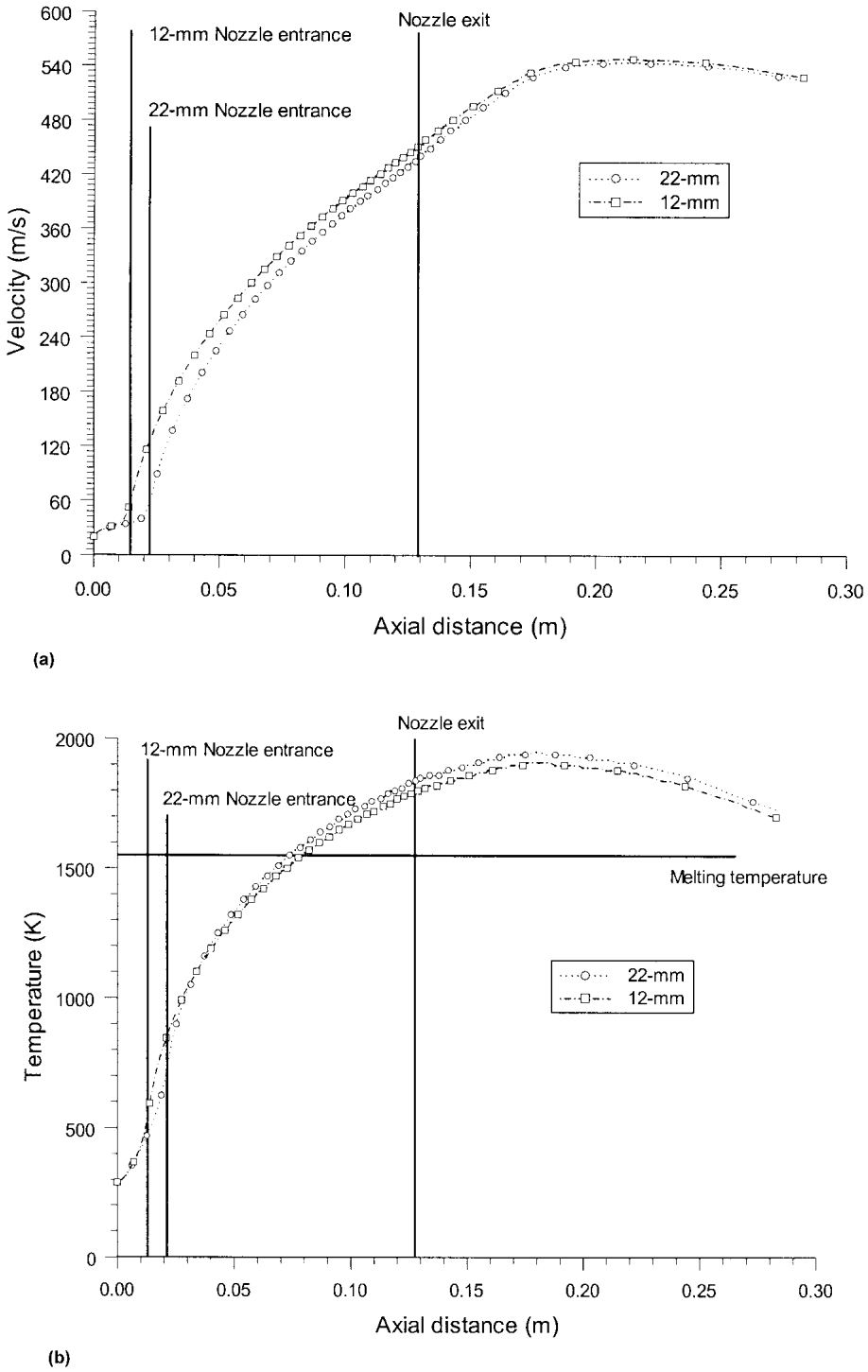

Fig. 8 **(a)** Evolution of particle velocity versus axial distance for different combustion chamber lengths (25 μm diameter particle). Total gas flow rate 705 SCFH, F/O ratio 0.27. **(b)** Evolution of particle temperature versus axial distance for different combustion chamber lengths (25 μm diameter particle). Total gas flow rate 705 SCFH, F/O ratio 0.27.

- The particle velocity and temperature variations along the axis of the gun principally depend on the total gas flow rate. The gas ratio has virtually no effect on the particle temperature profile and the increment of particle velocity at high fuel-to-oxygen ratio is mainly due to the increase of total mass flow rate due to the greater density of propylene when fixed volume flow rates are considered.
- The momentum and heat exchanges between small particles and gas flow are more efficient and, as a result, small par-

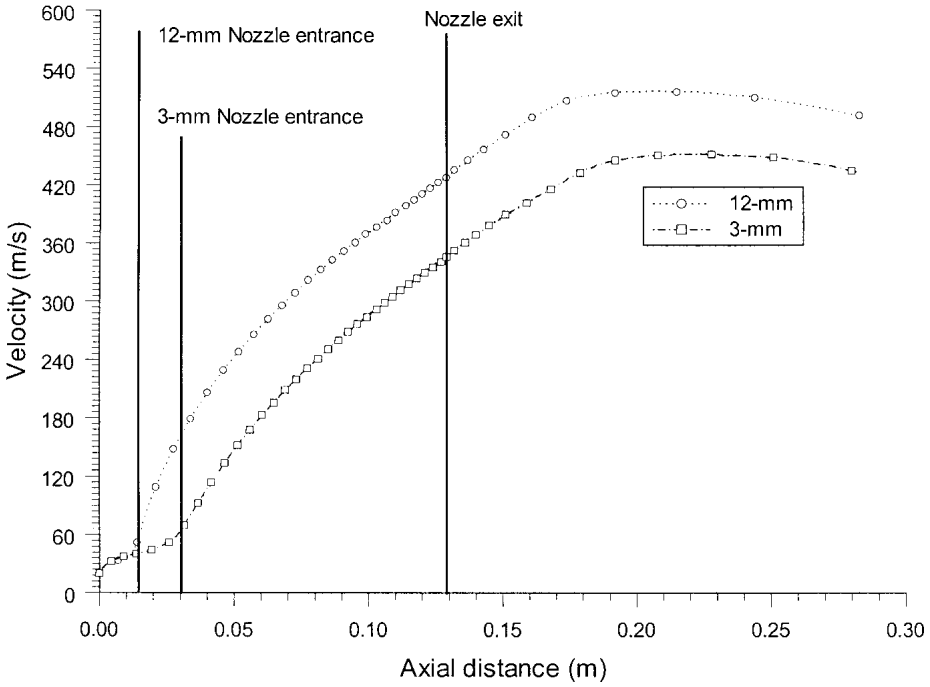

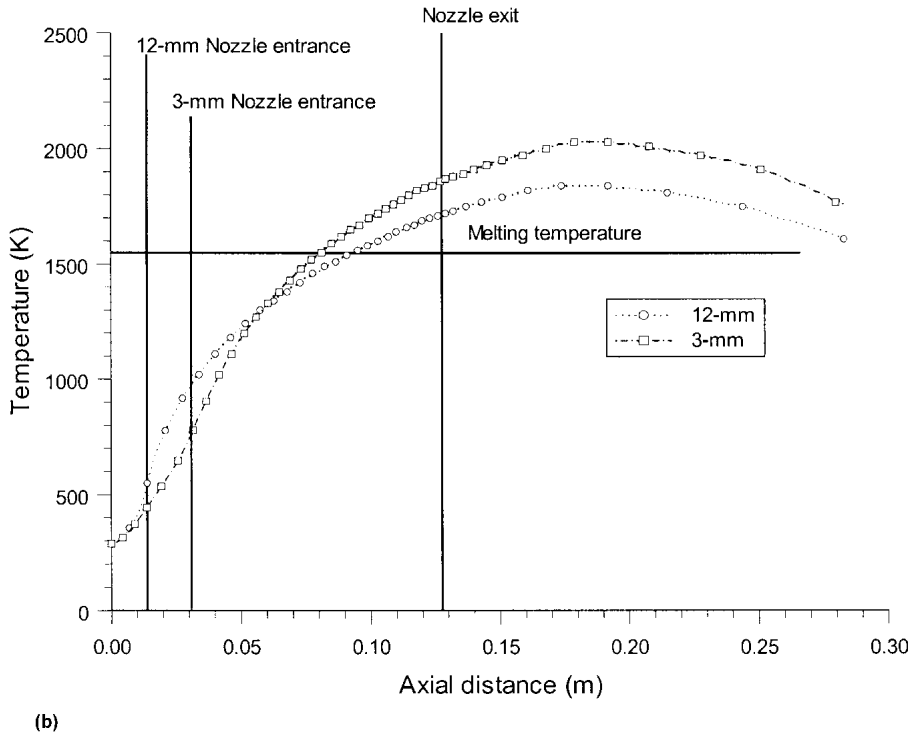

Fig. 9 **(a)** Evolution of particle velocity versus axial distance for different combustion chamber designs (25 μm diameter particle). Total gas flow rate 705 SCFH, F/O ratio 0.27. **(b)** Evolution of particle temperature versus axial distance for different combustion chamber designs (25 μm diameter particle). Total gas flow rate 705 SCFH, F/O ratio 0.27.

ticles are accelerated and heated effectively; whereas, larger particles are not during the spray process.

- The 22 mm chamber design of the gun is able to provide better particle heating with little change in velocity by increasing the particle dwell time.
- The 3 mm chamber design leads to significantly decreased

particle velocity and increased particle temperature. The conical convergent chamber may reduce the particle contact with the internal surface of the nozzle and hence decrease the potential for nozzle blockage with a low melting point material.

Acknowledgments

The authors acknowledge financial support for the study from BOC Gases UK and are grateful to Prof. T. Hyde, School of Mechanical, Materials, Manufacturing Engineering and Management, University of Nottingham for provision of laboratory facilities.

Appendix Table A1 Gas Flow Rate Conversions

Gas	SCFH	1 min^{-1}	m^{-3} s^{-1}	kg s^{-1}
C_3H_6	150	71	1.17×10^{-3}	2.26×10^{-3}
O_2	555	262	4.33×10^{-3}	6.24×10^{-3}
N_2	35	16.5	0.27×10^{-3}	0.344×10^{-3}

References

1. G.D. Power, E.B. Smith, T.J. Barber, and L.M. Chiapetta: "Analysis of a Combustion (HVOF) Spray Deposition Gun," UTRC Report No. 91-8, UTRC, East Hartford, CT, 1991.
2. E.B. Smith, G.D. Power, T.J. Barber, and L.M. Chiapetta: "Application of Computational Fluid Dynamics to the HVOF Thermal Spray Gun" in *Thermal Spray: International Advances in Coatings Technology,* C.C. Berndt, ed., ASM International, Materials Park, OH, 1992, pp. 805-810.
3. W.L. Oberkampf and M. Talpallikar: "Analysis of a High Velocity Oxygen-Fuel (HVOF) Thermal Spray Torch Part 1: Numerical Formulation," *J. Therm. Spray Technol.,* 1996, *5*(1), pp. 53-61.
4. W.L. Oberkampf and M. Talpallikar: "Analysis of a High Velocity Oxygen-Fuel (HVOF) Thermal Spray Torch Part 2: Computational Results," *J. Therm. Spray Technol., 5*(1), 1996, pp. 62-68.
5. B. Hassan, W.L. Oberkampf, R.A. Neiser, and T.J. Roemer: "Computational Fluid Dynamic Analysis of a High Velocity Oxygen-Fuel(HVOF) Thermal Spray Torch" in *Thermal Spray Science and Technology,* C.C. Berndt, ed., ASM International Materials Park, OH, 1995, pp. 193-98.
6. A.R. Lopez, B. Hassen, W.L. Oberkampf, R.A. Neiser, and T.J. Roemer: "Computational Fluid Dynamics Analysis of a Wire-Feed, High-Velocity Oxygen Fuel (HVOF) Thermal Spray Torch," *J. Therm. Spray Technol.,* 1998, *7*(3), pp. 374-82.
7. X. Yang and S. Eidelman: "Numerical Analysis of the High Velocity Oxygen-Fuel (HVOF) Thermal Spray (TS) System," *J. Therm. Spray Technol.,* 1996, *5,* pp. 175-84.
8. S. Gu, C.N. Eastwick, K.A. Simmons, and D.G. McCartney: "Computational Fluid Dynamic Modeling of Gas Flow Characteristics in a High-Velocity Oxy-Fuel Thermal Spray System," *J. Therm. Spray Technol., 10*(3), 2001, pp. 461-69.
9. Anon.: *CFX User's Manual,* CFX International, AEA Technology plc, Harwell, Oxon, UK, 1997.
10. L. Pawlowski: *The Science and Engineering of Thermal Spray Coatings,* John Wiley & Sons, Chichester, West Sussex, UK, 1995.
11. E. Bourdin and P. Fauchais: "Transient Heat Conduction Under Plasma Conditions," *Int. J. Heat Mass Transfer,* 1983, *26*(4), pp. 567-82.
12. V.J. Shrikant and R. Sivakumar: "Particle Behaviour During High Velocity Oxy-Fuel Spraying," *Surf. Coat. Technol., 50,* 1991, pp. 67-74.
13. H. Edris, D.G. McCartney, and A.J. Sturgeon: "Microstructural Characterisation of High Velocity Oxy-fuel Sprayed Coatings of Inconel 625," *J. Mater. Sci.,* 1997, *32,* pp. 863-72.